Neural Networks 163 (2023) 97–107

Contents lists available at ScienceDirect

Neural Networks

journal homepage: www.elsevier.com/locate/neunet

An explainable artificial intelligence approach to spatial navigation based on hippocampal circuitry

Simone Coppolino, Michele Migliore *

Institute of Biophysics, National Research Council, Palermo, Italy

ARTICLE INFO

Article history:
Received 19 April 2022
Received in revised form 30 January 2023
Accepted 21 March 2023
Available online 30 March 2023

Keywords:
Robot spatial navigation
Spike-time-dependent plasticity
Hippocampal circuitry
Spiking neurons network

ABSTRACT

Learning to navigate a complex environment is not a difficult task for a mammal. For example, finding the correct way to exit a maze following a sequence of cues, does not need a long training session. Just a single or a few runs through a new environment is, in most cases, sufficient to learn an exit path starting from anywhere in the maze. This ability is in striking contrast with the well-known difficulty that any deep learning algorithm has in learning a trajectory through a sequence of objects. Being able to learn an arbitrarily long sequence of objects to reach a specific place could take, in general, prohibitively long training sessions. This is a clear indication that current artificial intelligence methods are essentially unable to capture the way in which a real brain implements a cognitive function. In previous work, we have proposed a proof-of-principle model demonstrating how, using hippocampal circuitry, it is possible to learn an arbitrary sequence of known objects in a single trial. We called this model SLT (Single Learning Trial). In the current work, we extend this model, which we will call e-STL, to introduce the capability of navigating a classic four-arms maze to learn, in a single trial, the correct path to reach an exit ignoring dead ends. We show the conditions under which the e-SLT network, including cells coding for places, head-direction, and objects, can robustly and efficiently implement a fundamental cognitive function. The results shed light on the possible circuit organization and operation of the hippocampus and may represent the building block of a new generation of artificial intelligence algorithms for spatial navigation.

1. Introduction

During the exploration of an unknown environment, such as a building, a museum or, more generally, a maze, we usually wander around walking from one point to another following a sequence of cues that generated some interest, eventually reaching an exit. This process could take more or less time depending on several factors such as the size and/or complexity of the environment, orientation ability, special conditions, etc. However, all these factors do not influence our ability to reach the exit after very few, most often just one, navigation period. The hippocampus is the brain region most involved in this cognitive function. Although the involved circuits are not completely understood, there are clear experimental findings, *in vitro* and *in vivo*, demonstrating the existence, in the CA1 region of the hippocampus, of cells selectively responding to specific locations with respect to external cues (O'Keefe & Dostrovsky, 1971), to specific head directions (Leutgeb, Ragozzino, & Mizumori, 2000), or specific objects (Quiroga, Reddy, Kreiman, Koch, & Fried, 2005). The spatial navigation function appears to be implemented using these types of cells, exquisitely tailored and wired to form microcircuits from which it naturally emerges. Our ability and efficiency in learning to navigate a new environment and remember the path to exit, is currently not achievable by any robot or device using state-of-the-art artificial intelligent algorithms, such as Long Short-Term Memory or Bidirectional Recurrent neural networks.

In recent years, a new paradigm is emerging, to build neural networks able to somewhat replicate human cognitive functions: the eXplainable Artificial Intelligence approach (XAI, reviewed in Gunning et al., 2019), a way to implement models in which the rationale and the steps leading to the emergence of a cognitive function are well defined. This is achieved by using neurobiologically plausible network architectures (reviewed in Zeno, Patel, & Sobh, 2016), which allows a clear characterization of their strengths and weaknesses and, most importantly, allows to entirely understand and predict their behavior under different conditions. Following this approach, robot navigation systems have been built to create a cognitive spatial map of the environment to learn how to reach a target. However, to the best of our knowledge, in all cases the learning phase still crucially depends on reinforcement learning schemes based on Q-learning rules (Arleo & Gerstner, 2000; Sutton & Barto, 2018). A recently published model, inspired by hippocampal circuitry and casted

* Corresponding author.
E-mail address: michele.migliore@cnr.it (M. Migliore).

https://doi.org/10.1016/j.neunet.2023.03.030

in terms of spatial and relational memories, achieved impressive results (e.g. Whittington, Warren, & Behrens, 2021; Whittington et al., 2020). However, the model still relies on long and very specific training sessions to learn enough transitions in a graph representing the environment, in such a way to efficiently find a correct path to the desired location.

More generally, all current models require the evaluation of a cost function that depends on the actual target's location, with learning schemes that systematically rely on algorithms that need the calculation (and backpropagation) of an error (based on energy functions, distance from special locations, specific sequences, etc.) with respect to a "true" configuration. This is in striking contrast with what happens *in vivo*, where the target location and the sequence of objects to follow to reach it are unknown. A notable exception is the *eligibility traces* approach (e.g. Strösslin, Sheynikhovich, Chavarriaga, & Gerstner, 2005), where the system (implemented as a set of interacting networks composed by several hundred neurons) achieves one-shot learning by keeping a non-decaying memory of the complete state–action history at each step.

In the current work, we build upon the SLT model, a previously published spiking neuron network based on hippocampal cells and circuits (Coppolino, Giacopelli, & Migliore, 2022), to introduce the e-STL model. Place Cells, Head Direction Cells, and other neuron types are wired together with plastic synapses to form a self-organizing network able to learn, in a single learning trial, the correct sequence of objects to follow toward an exit. The learning process is controlled by a spike-time-dependent plasticity rule, with excitatory and inhibitory neurons modulating the appropriate learning/forgetting process during the exploration of the environment, without the use any type of cost function. The new e-SLT network is able to control the navigation of a robot exploring a maze, and it makes experimentally testable predictions on the physiological mechanisms underlying this function in humans and other mammals. The results suggest a new generation of explainable artificial intelligence algorithms for spatial navigation.

2. Methods

All model and simulation files will be publicly available on ModelDB (http://modeldb.yale.edu/267339). The network was implemented in PYNN (Davison et al., 2009), and the Robot Operating System (ROS,www.ros.org) was used to build a basic closed-loop environment using external inputs to control the movement of a virtual robot Several python custom transfer functions were also implemented to integrate the PYNN and ROS code with the NeuroRobotics Platform of the Human Brain Project (HBP-NRP, https://neurorobotics.net/). To compare the performance of our network with a Long-Short-Term-Memory (LSTM) recurrent network (Schmidhuber, 2015), we used a previously published code (Brownlee, 2018). We used the vanilla LSTM implemented with Keras (Chollet, 2015) and Tensor Flow (Abadi et al., 2015), with some changes to make it more similar to the neuronal model, and ensure a fair comparison of the performances. The test was focused on the ability of the LSTM network to remember and forget numerical sequences with different rules (i.e. +1, +2, +3 and +4 sequences rule). In this way, the LSTM network does not need to learn any external features since only the training sequences are presented to the model.

2.1. Network components and connectivity

The network is schematically shown in Fig. 1; it is an extension of the one used to introduce the basic concepts and a proof of principle of operations (Coppolino et al., 2022). It is composed of both excitatory and inhibitory cells, with computational properties consistent with those observed in the hippocampus and described below. In adding interneurons, the hyper-parameters needed to be re-tuned, with respect to the previous version. It should be noted that, as it can be expected and as it actually works in real biological systems, thanks to the degeneracy phenomenon, essentially the same result can be obtained with many combinations of parameters (e.g. Migliore, Novara, & Tegolo, 2008). The main mechanism is the appropriate self-organization of the synapses, which relies on the interplay between pre- and post-synaptic firing rates. We choose the latter to be in the theta-gamma frequency range (approximately 4–80 Hz), experimentally observed during cognitive functions. As long as the various neurons and synaptic parameters are able to generate firing rates in this range, which will activate synapses' potentiation and depression as described in the Results Section, the network will work independently of environment's shape or size, with the limitations described in the Discussion Section.

A key point of this new architecture is the inclusion of interneurons, which are a fundamental component of any real brain region. Excitatory neurons were tuned to selectively firing in the presence of different objects or different head directions, and neurons firing persistently in response to a specific input. These properties were hard coded in the input pathways, in such a way that each cell would receive only the part of the input consistent with its tuning, as result of a previous learning process that was given for granted in this work. No specific assumptions were made for the tuning of inhibitory neurons. Finally, we used our intuition and experimental suggestions to connect the network, as described below. We found that a fully functional network can be implemented using a number of interneurons much smaller that the excitatory neurons, in agreement with experimental findings. For the purpose of this paper, we used 46 leaky integrate-and-fire (LIF) neurons, 35 excitatory and 11 inhibitory, recognizing 5 objects and 12 head directions (30 degrees steps). They represent the following cell types:

- *Object cells (OBJ)*, which selectively fire when an object with a specific feature is in the visual field. In our case, the key feature is a color. The explicit tuning of individual hippocampal neurons to specific objects has been observed experimentally (Quiroga et al., 2005), and we have previously shown how this can be implemented using a biophysically detailed single cell model (Migliore et al., 2008).
- *Persistent Firing (PF)* neurons, activated as an OBJ neuron but with a delay. Consistent with experimental findings (Boran et al., 2019), their firing persists when the relative object is not present anymore and continues firing until another PF starts firing. This feature was implemented using autapses. Although they are not usually investigated in detail, autapses are very common in the brain. Their presence has been confirmed in the neocortex (Lübke, Markram, Frotscher, & Sakmann, 1996; Van der Loos & Glaser, 1972), in the olfactory bulb (Schoppa & Westbrook, 2002) and in the hippocampus (Franck, Pokorny, Kunkel, & Schwartzkroin, 1995; Knopp, Kivi, Wozny, Heinemann, & Behr, 2005). As for *OBJ* neurons, at any given time only one PF neuron is active
- *Head Direction/Place Cells, HD/PC*, activated when the animal/robot's head is pointing at a specific spatial location (*HD*); their coding evolves with experience and, during the learning phase, some of them may become Place Cells (*PC*). They can thus represent not only space but also contextual information (Gulli et al., 2020). For this reason, we will alternatively refer to them as *HD* or *PC* cells. As for *OBJ* and *PF* neurons, only one *HD/PC* neuron is active at any given time. These cells are a hallmark of spatial navigation and are commonly found in the CA1 hippocampal region (Danjo, 2020).

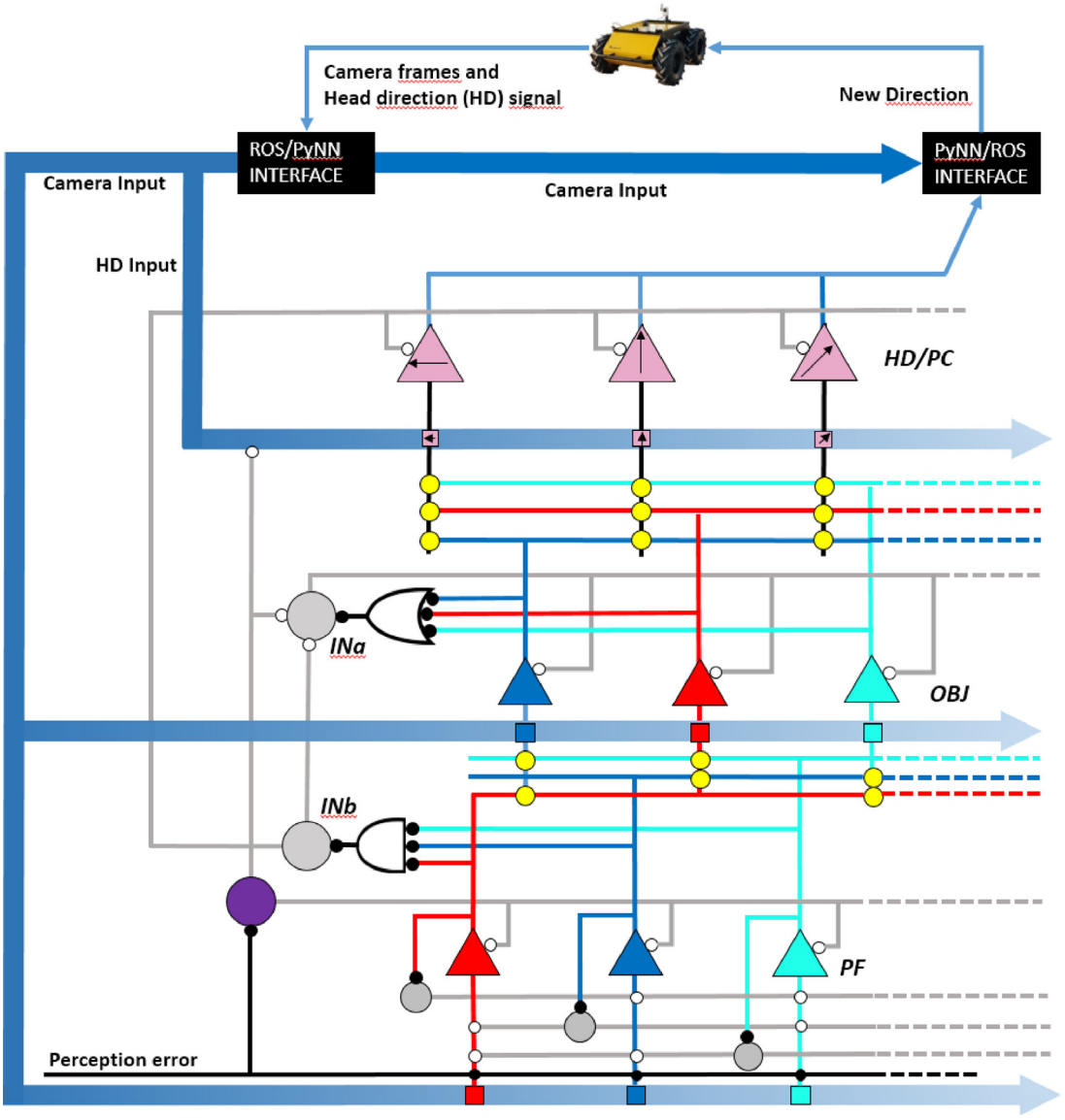

Fig. 1. Schematic representation of the Network. **Colored triangles** represent excitatory neurons tuned to objects of different colors or different head directions; **gray or purple circles** represent interneurons; **thick blue lines** represent inputs from the robot, carrying contextual information (object color and current Head Direction); **colored squares** on the thick blue lines indicate that the relative cell will be activated whenever the corresponding information is present in the input stream; OBJ, Object cells; PF, Persistent Firing cells; HD/PC, Head Direction/Place Cells; synaptic connections are represented with small circles, following the conventional color for excitatory (black) or inhibitory (white); excitatory plastic synapses are indicated in yellow; the **Perception error** is an external signal, activated by a dead-end. Lines fading or turning dashed in the right part of the scheme represent the network modularity.

- *Interneurons, INa-b,* making inhibitory connections with OBJ, HD/PC, and PF neurons. Consistently with a real hippocampal network, their overall number was significantly lower than the excitatory neurons (Aika, Ren, Kosaka, & Kosaka, 1994; Woodson, Nitecka, & Ben-Ari, 1989).

The network has two input lines (*Camera* and *HD* thick blue paths in Fig. 1): one carrying information on the robot's head direction, and one on the visual field. Camera frames and head direction information are continuously transmitted by the robot and are analyzed by the ROS/PYNN interface, which extracts information on the presence of shapes of specific colors and sends this information to the *OBJ* and *PF* neurons. Only the neuron coding for the specific object will be activated. Analogously, only the *HD* neuron coding for the specific head direction will be activated. The *OBJ* neurons are connected with *HD/PC* neurons through plastic synapses. Any active *OBJ* neuron will generate a feedback and lateral inhibitory signal through a static synapse, in a logic OR connection onto interneuron *INa*. This type of circuit organization is ubiquitous in the brain, from the olfactory bulb (Yokoi, Mori, & Nakanishi, 1995) to the hippocampus (e.g. Ferrante, Migliore, & Ascoli, 2009), and it forms the basis for powerful computational properties. The *PF* neurons make synaptic contacts with all *OBJ* neurons coding for objects different from their own (e.g. the blue *PF* does not have a synapse with the blue *OBJ* neuron). Through a logic AND connection, they may activate interneuron *INb*. HD/PC neurons receive independent excitatory inputs from all OBJ neurons, a common inhibitory input from PF neurons, and their HD input is modulated by an interneuron activated by the Perception error signal.

For the sake of simplicity, all neurons had the same electrophysiological properties. Using a typical LIF conductance-based implementation (Cessac & Viéville, 2008; Nordlie, Tetzlaff, & Einevoll, 2010), the membrane potential v(t) of a neuron in a

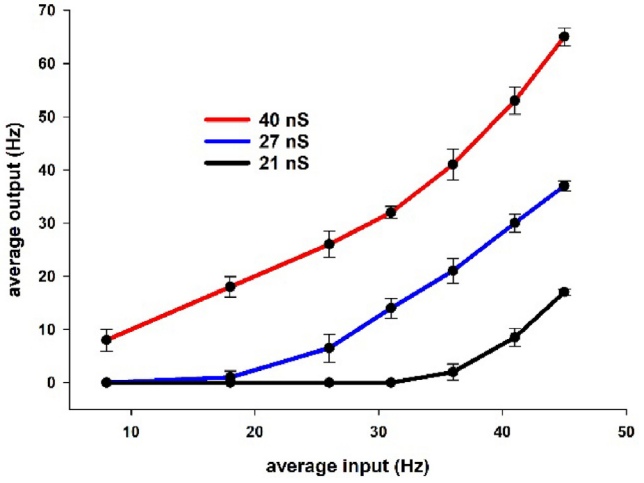

Fig. 2. Input/Output properties of neurons. Average (n=10) response of a neuron to a random 1 s synaptic activation at different average frequencies and peak synaptic weights.

subthreshold regime (i.e. for $v(t) < V_{th}$), is described by

$$\tau_m \frac{dv(t)}{dt} = -v(t) + R_m \cdot \left[g^E_{syn}(t) \left(v(t) - E^E_{syn} \right) + g^I_{syn}(t) \left(v(t) - E^I_{syn} \right) \right] \quad (1)$$

Where $\tau_m = 20$ ms is the membrane time constant, $R_m = 20\ m\Omega/cm^2$ is the specific membrane resistance, and $V_{th} = -50$ mV is the spike threshold. Each time, t_k, at which $v(t)$ crosses V_{th}, it is: $\forall k: t \notin (t_k, t_k + \tau_{ref}]$, $v(t) = V_{reset}$ where, $V_{reset} = -65.0$ mV, $E^E_{syn} = 0$ mV for excitatory input, $E^I_{syn} = -70.0$ mV for inhibitory input, and $\tau_{ref} = 1.0$ ms is the refractory period. The $g_{syn}(t)$ indicates the synaptic excitatory or inhibitory inputs. Synaptic activation times were implemented with Poisson spike generators (Brette, Rudolph, Carnevale, et al., 2007; Brunel, 2000). In the rest of this section, $\eta(\nu)$ indicates a random variable used to generate spike times according to a Poisson distribution (Johnson, Kemp, & Kotz, 2005), at an average frequency ν. In Fig. 2, we report the response of a neuron for a series of simulations in which a random (Poisson) synaptic input was activated for 1 s at different average frequencies and peak synaptic weights, with 10 repetitions. The average output firing frequency covered the main spectrum of experimentally observed brain rhythms in hippocampal principal neurons during behavioral tasks, up to the high gamma range (~80 Hz).

2.2. Coding of input cues

The number, n_{obj}, of pixels in a given frame arriving from the robot camera, was used to generate a train of synaptic activations on the Persistent Firing cells (*PF*), Object cells (*OBJ*) and some Interneurons (*INT*), with a Poisson process with an average frequency defined as

$$\eta_{obj} = 25 \cdot \left(e^{-\left(\frac{n_{obj}-\mu}{\sigma}\right)^2} \right) \quad (2)$$

where $\mu = \{0.055\}$, and $\sigma = \{0.07\}$ for red, blue, black, green, purple, magenta and cyan input sensor. This formulation allowed us to consider the feedback inhibition during strong inputs, a feature present at different levels in the retina circuitry (Diamond, 2017). Synaptic inputs coding for 18 different Head Directions (HD_i, considering 20 degrees of visual field) were also implemented as Poisson processes as:

$$\eta_{HD_i} = \begin{cases} \eta(\nu_{HD}), & if\ state\ HD_i \\ 0, & otherwise \end{cases} \quad (3)$$

with $\nu_{HD} \cong 20.0$ Hz and weight 0.05 μS. Each *PF* neuron was activated only by one object, and for each *obj* we can thus define the variable:

$$\eta_{PF} = \eta_{obj}$$

The same for each HD/*PC* neuron, which was activated only by one HD_i

$$\eta_{PC} = \eta_{HD_i}$$

The equations describing the dynamics of the membrane potential for each type of neuron (*PF*, *obj*, *PC*) can be thus written as follows. For *PF* cells, defining $d_{INT,PF}$ as 1 if *INT* and *PF* are such that $\eta_{Int} = \eta_{PF}$ and 0 otherwise, is

$$\tau_m \frac{dV_{PF}(t)}{dt} = -V_{PF}(t) + R_m \left\{ \left(g^{\eta_{PF},PF}_{syn} + g^{PF,PF,E}_{syn} \right) \left(V_{PF}(t) - E_{syn}{}^E \right) + \left(\sum_{Int_1} (1 - d_{Int_1,PF}) g^{Int_1,PF}_{syn} + g^{PF,PF,I}_{syn} + g^{Int_2,PF}_{syn} \right) \left(V_{PF}(t) - E_{syn}{}^I \right) \right\}$$

where

$$g^{\eta_{PF},PF}_{syn}(t) = w_{\eta_{PF},PF} \sum_k \delta(t - t_{k,E}) e^{-\frac{(t-t_{k,E})}{\tau}},$$

$$g^{PF,PF,E}_{syn} = w_{\eta_{PF},PF,E} \sum_k \delta(t - t_{k,E}) e^{-\frac{(t-t_{k,E})}{\tau}},$$

$$g^{PF,PF,I}_{syn} = w_{\eta_{PF},PF,I} \sum_k \delta(t - t_{k,I}) e^{-\frac{(t-t_{kI})}{\tau}},$$

$$g^{Int_1,PF}_{syn}(t) = w_{Int_1,PF} \sum_k \delta(t - t_{k,I}) e^{-\frac{(t-t_{k,I})}{\tau}},$$

and $g^{Int_2,PF}_{syn}(t) = w_{Int_2,PF} \sum_k \delta(t - t_{k,I}) e^{-\frac{(t-t_{k,I})}{\tau}}$ when $\eta_{obj} = \eta_{purple}$ (η_{purple} is associated to a purple object that indicates a dead-end) $w_{x,y}$ is the peak conductance of the synapse connecting neurons x and y, $\tau = 5.0$ ms and the synaptic activation times t_k were generated according to η_{PF}. For *obj* cells, defining $d_{PF,obj}$ as 1 if *PF* and *obj* are such that $\eta_{PF} = \eta_{obj}$ and zero otherwise, the equation is:

$$\tau_m \frac{dV_{obj}(t)}{dt} = -V_{obj}(t) + R_m \left[\left(g^{\eta_{obj},obj}_{syn} + \sum_{PF} \left(1 - d_{PF,obj}\right) g^{PF,obj}_{syn} \right) \times \left(V_{obj}(t) - E_{syn}{}^E \right) + g^{Int,obj}_{syn} \left(V_{obj}(t) - E_{syn}{}^I \right) \right],$$

with $g^{PF,obj}_{syn}(t) = w_{PF,obj} \sum_k \delta(t - t_{k,E}) e^{-\frac{(t-t_{k,E})}{\tau}}$, $g^{Int,obj}_{syn}(t) = w_{Int,obj} \sum_k \delta(t - t_{k,I}) e^{-\frac{(t-t_{k,I})}{\tau}}$ and the synaptic activation times $t_{k,E}$ were the spike times of the corresponding *PF* cell. Moreover,

$$g^{\eta_{obj},obj}_{syn}(t) = w_{\eta_{obj},obj} \sum_k \delta\left(t - t_{k,E}\right) e^{-\frac{\left(t-t_{k,E}\right)}{\tau}}$$

where the synaptic activation times $t_{k,E}$ are generated according to η_{obj}. For HD/*PC* neurons,

$$\tau_m \frac{dV_{PC}(t)}{dt} = -V_{PC}(t) + R_m \left[\left(g^{\eta_{PC},PC}_{syn} + \sum_{obj} g^{obj,PC}_{syn} \right) \right.$$

$$\times \left(V_{PC}(t) - {E_{syn}}^{E}\right) + g_{syn}^{Int,PC} \left(V_{PC}(t) - {E_{syn}}^{I}\right)\Bigg],$$

where

$$g_{syn}^{obj,PC}(t) = w_{obj,PC} \sum_k \delta(t - t_{k,E}) e^{-\frac{(t-t_{k,E})}{\tau}},$$

with the synaptic activation times t_k defined by the spike times of the *OBJ* cells, and

$$g_{syn}^{\eta_{PC},PC}(t) = w_{\eta_{PC},PC}\left(\sum_k \delta\left(t - t_{k,E}\right) e^{-\frac{\left(t-t_{k,E}\right)}{\tau}}\right)$$

where the synaptic activation times t_k were generated according to η_{PC}.

2.3. Synaptic plasticity rule

During the learning phase, the synaptic weight between any two neurons, w_{ij}, evolved following an asymmetric spike-time-dependent synaptic plasticity rule (STDP), implemented by considering experimental findings in the hippocampus (Nishiyama, Hong, Mikoshiba, Poo, & Kato, 2000) as:

$$\Delta w_{ij} = 0.2e^{\left(-\frac{x}{13}\right)} \quad \text{for } x > 0 \tag{4}$$

$$\Delta w_{ij} = -0.12e^{\left(\frac{x}{30}\right)} \text{ for } x < 0 \tag{5}$$

where $x = t_j - t_i$, and $\{t_i, t_j\}$ were the pre and post synaptic spike times, respectively.

The initial weights were set to 0.007 μS and were allowed to reach a peak conductance of 0.04 μS.

2.4. Virtual spatial environment

For all simulations we used the same virtual environment, shown in Fig. 3, created using the EBRAINS Neurorobotics Platform (https://neurorobotics.net/). We have chosen a four-arms maze, as this is the most common environment used in experimental investigations of spatial navigations. Objects were randomly placed over the entire space, with the exceptions of those representing key locations such as an exit (green object), dead ends (light purple), and the starting point (dark purple). The results discussed in the next sections did not change using highly different object locations and size, and by changes in the configuration of the test maze.

3. Results

3.1. Network operation during learning

The different steps during a typical learning phase are illustrated in Fig. 4, where the portion of the network involved in each step is highlighted

(1) The robot starts searching for a known object; eventually it sees a known object, in this case the blue one; it thus starts moving toward it, and the blue OBJ neuron starts firing; during the exploration, the HD input selectively activates the HD/PCs corresponding to the current robot's head direction. The circuitry involved in this step is schematically highlighted in Fig. 4A.
(2) The blue OBJ activity is propagated to: (a) an interneuron, generating lateral and feedback inhibition onto all OBJs, a classic contrast enhancement effect (Yokoi et al., 1995) and, (b) to all the HD/PCs; this latter input, associated with the postsynaptic firing of the only HD/PC neuron activated by the current HD signal (step 1), will induce long-term potentiation of the blue OBJ-HD/PC synapse (schematically represented with a larger light-yellow circle in Fig. 4A).
(3) As the robot approaches the blue object, the corresponding input increases and eventually enters the desensitization phase (see Eq. (2)). At this point, the robot begins to look around for other known objects, it detects the red, yellow and black objects; it randomly chooses to follow one of them, excluding those already explored; in this case it chooses the red one, and it marks it as already explored, for future reference.
(4) Meanwhile, the blue *PF* neuron will also begin to generate spikes, which are propagated to all other *OBJ*s, and to another interneuron exerting lateral inhibition on all the other *PF*s.
(5) The circuitry involved in this step is highlighted in Fig. 4B. The red *OBJ* cell increases its firing as the robot approaches the red object; together with the presynaptic activity generated by the blue *PF* neuron this results in the bluePF-redOBJ synapse being potentiated (larger light-yellow synapse in Fig. 4B).
(6) Steps (2), (3), and (4) are then repeated until the robot sees an exit or the network receives a *Perception error* signal, in our case coded by a magenta object and corresponding to a dead end. In the first case, the learning phase is complete; the appropriate synapses have been potentiated to direct the movement of the robot through the sequence of objects leading to the exit.
(7) The *Perception error* input, lasting until the robot goes back to the starting point, puts the network into the forgetting cycle, which has two phases: (1) direct activation of all *PF*s, (2) delayed activation of an interneuron that inhibits all *PF*s and reduces activation of *HD/PC*s; the circuitry involved in the first phase is schematically shown in Fig. 4C; while the robot reaches the dead end (magenta object), all the *PF*s neurons are active at the same time; their activity removes lateral inhibition from *OBJ*s, which will thus be strongly activated. The resulting large difference between the pre- and postsynaptic firing in *OBJ*s creates the conditions for synaptic depression (post-synaptic spikes in most cases anticipate presynaptic spikes), and the previously potentiated

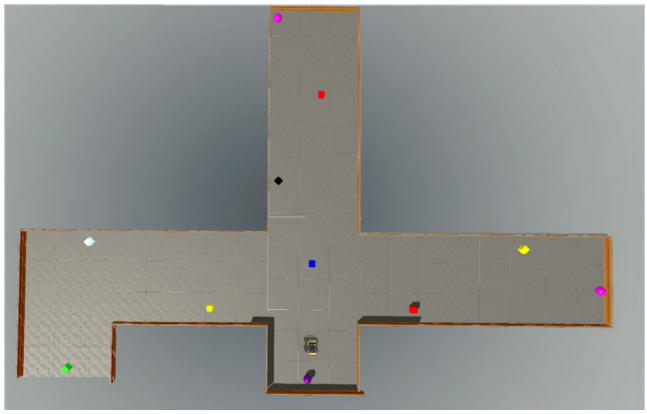

Fig. 3. The virtual environment used for all simulations. Object locations are random, except for the purple objects on the right and top arms, which represent dead ends, and the green object on the left arm, which represents an exit. The rover starts exploring the maze from the dark purple object in the lower arm.

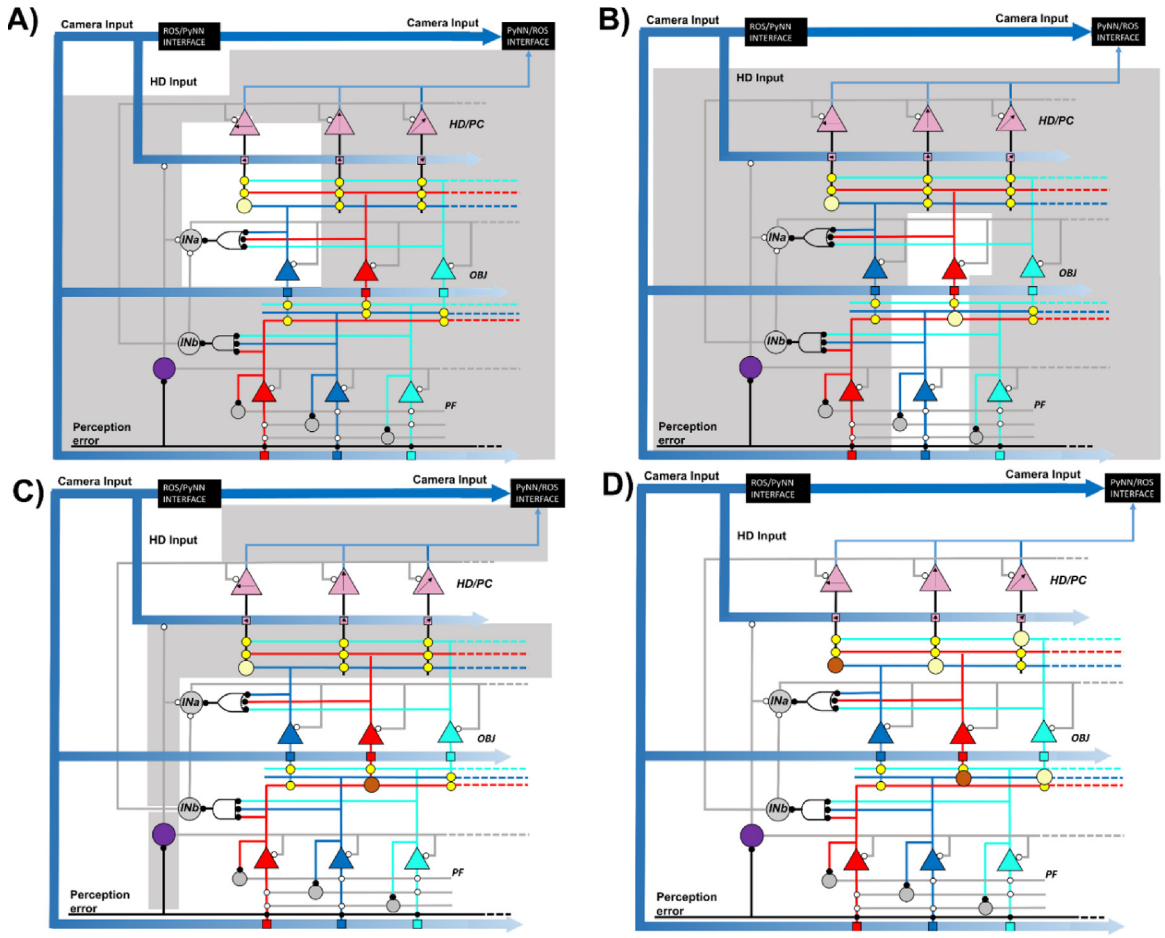

Fig. 4. Schematic representation of the portion of the network involved in the different steps during a learning cycle. Each panel highlights the portion of the network most active at different times during the exploration of the maze. **(A)** The robot sees a blue object; the blue OBJ neuron starts firing and activates interneuron INa (through the OR gate); the HD/PCs cell, corresponding to the current head direction, is also firing, and this potentiated the blue OBJ-HD synapse (larger light yellow circle). **(B)** the blue object exits the field of view and a red object appears; the blue PF neuron will begin to generate spikes, together with the red OBJ cell, and the bluePF-redOBJ synapse will be potentiated (larger light-yellow synapse). **(C)** when the robot sees a dead-end signal, the Perception error input activates all the PFs neurons; their combined activity (AND gate) removes lateral inhibition from OBJs, by activating the INb interneuron and consequently inhibiting INa; the previously potentiated PF-OBJ synapse is depressed (dark-orange synapse). **(D)** As the robot starts returning back, essentially the entire network will be active; the purple interneuron, activated by the Perception error signal (with a delay), generates feedback inhibition on all PFs and feed-forward inhibition onto all HD/PCs through the purple interneuron. In the meanwhile, all OBJ cells are firing, because their inhibition is blocked; their relative firing results in the depression of all the previously potentiated synapses on HD/PC cells; the robot eventually reaches the starting position, the Perception Error is reset and the learning process could continue; the final weights' configuration, for this specific maze and object locations, are represented with color-coded circles (dark orange and light yellow).

PF-OBJ connections will be depressed (dark-orange synapse in Fig. 4C).

(8) As the robot begins to look for other objects, the interneuron activated by the error signal begins to fire and *PF*s will be inhibited. During its backward navigation, the robot will see all the objects that it has just learned. However, this time all *OBJ* cells are firing because feedback and lateral inhibition is blocked; an *OBJ* input, and the previously potentiated *OBJ-HD/PC* synapse result in these latter neurons to fire at higher frequency; as before, this condition will set the stage for synaptic depression. Following this process, the network will forget the association between a *HD/PC* and an *OBJ* neuron. Eventually, the robot reaches the starting position, the *PF* error is reset, and the learning process could restart in another branch; the final weights' configuration, for this specific maze and object locations, is shown in Fig. 4D; synaptic weights (dark orange and light yellow in Fig. 4D) reflect the objects and directions that the robot has followed to reach the exit.

3.2. Recallphase

During the learning phase, the network has self-organized its synapses during the process of finding an exit path. The end result was that selected *PF-OBJ* and *OBJ-HD/PC* synaptic weights have been potentiated or depressed, with respect to their initial value. The consequent *HD/PC*s firing pattern that will be generated as the robot enters the same maze at any point, can be used by the PyNN/ROS interface to control the robot's movement toward the exit, without any wrong turn. In this phase, the robot's movement will be entirely controlled by the potentiated *OBJ-PC* synapses, and it will directly follow the correct path, as soon as it sees any object belonging to the sequence that it has learned.

A movie of the simulation corresponding to the steps described above is available as Supplementary Movie 1. To test the robustness of the process, we repeated three times the learning

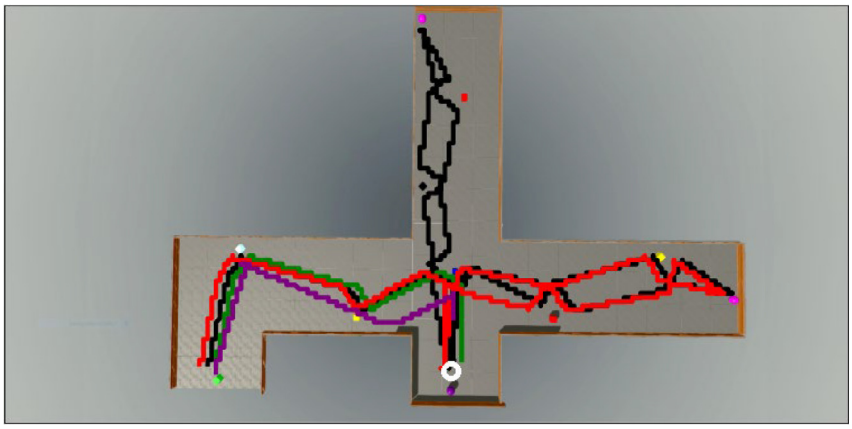

Fig. 5. Robustness of the Learning and Recall process. Red, Green, and Black traces represent the different paths explored by the robot during three different learning trials. The Purple line represents the recall path after each of them. The white marker represents the robot's starting position.

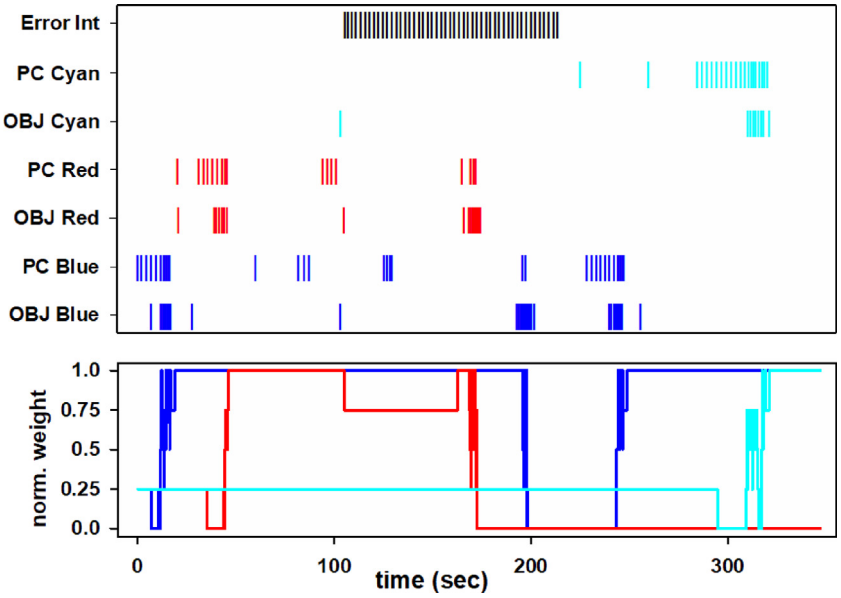

Fig. 6. Network dynamics during a typical learning trial. Raster plot of selected OBJ, and HD/PC neurons (top) and OBJ-HD/PC synaptic weight dynamics (bottom) during a typical learning/forgetting phase.

phase using the same objects' configuration in the maze but different random seeds for the Poisson processes and random choices on directions to follow at the maze junction. In Fig. 5 we show the paths followed by the robot for each case (red, green, and black traces in Fig. 5). For all of them, the robot was able to learn the path to the exit (purple trace in Fig. 5) in a single exploration trial. The same overall result was obtained using different objects' configuration or maze sizes and/or geometries (not shown).

It should be noted that it is not possible to make a direct comparison with the previous STL model (Coppolino et al., 2022), which was implemented to introduce the basic network architecture and demonstrating a proof of principle; in contrast with the e-STL model, it would not be able to successfully navigate a more realistic environment such as a 4-arms maze, because during the learning phase the network would keep potentiating synapses connecting sequential objects, independently from being in a wrong path, affecting in most cases the successful completion of the task.

To compare this performance with a network using a different architecture, we trained a LSTM network to test the capability of the forget gate to self-organize the synaptic weights, by progressively adding one object at the time, up to four sequences, as in our model. We found (see supplementary Fig.S1) that the network needed more than 3000 learning epochs to obtain an accurate result.

In Fig. 6 we show more details on the process underlying the network self-organization, where we show the spiking activity of specific neurons and the consequent potentiation or depression of the activated synapses.

For the sake of simplicity, we will discuss the process for a few *OBJ* and *HD/PC* neurons and their synapses. All others will follow the same conceptual time course. As discussed in the *Learning* Section (step 1), when the robot approaches the blue object, the corresponding neuron will begin to fire (OBJ Blue raster in Fig. 6, around t=15 s).

The conjunctive firing with one of the *HD/PC* neurons (PC Blue raster in Fig. 6) will selectively potentiate the corresponding synaptic weight (blue trace in bottom plot of Fig. 6). The same occurs as soon as the robot sees the red object, around t=40 s In this case, the association of the *OBJ* cell coding for the red object (OBJ Red in Fig. 6) and the cell coding for the current *HD*

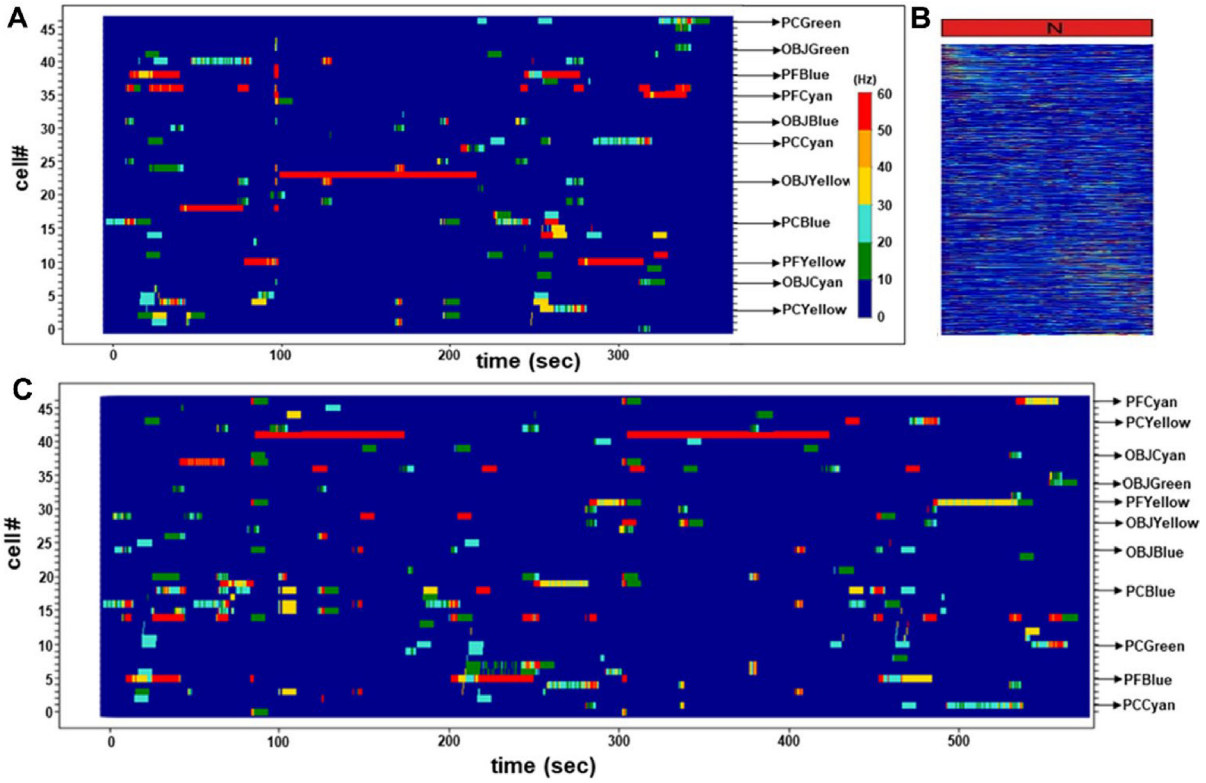

Fig. 7. Network dynamics during two typical learning trials. (A) Instantaneous firing rates, as a function of simulation time, for all cells in the network during an independent maze explorations. Cells' order is random. PC, PF, and OBJ neurons involved in the correct exit path are identified on the right. **(B)** Typical experimental finding, showing activation of cells with Place and Non-Place-Related activity during a run in a non-familiar (N) environment, from Dong, Madar, and Sheffield (2021). **(C)** As in A but for a different trial.

(PC Red in Fig. 6) potentiate their synaptic weight (red trace in Fig. 6). Note that red and blue *OBJ* neurons are different cells, but the *HD/PC* neuron involved in this process may or not be the same. In any case, the potentiated synapse will be different, even if the *HD/PC* cell is the same neuron that was activated in the presence of the blue object. This homosynaptic plasticity, a fundamental process of brain self-organization, is ensured by the mutually exclusive activation of an *OBJ* cell during the learning phase. As the robot proceeds with its navigation (50<t<100 s in Fig. 6), the weights remain constant

When the robot reaches a dead end, the (external) perception error signal will activate the purple interneuron (ErrorInt in Fig. 6). On its way back, the robot sees the red object again. However, in this phase (*Learning* Section step 9) the *HD/PC* cells are receiving a much stronger input from the (disinhibited) OBJ Red cell and the potentiated OBJ Red-PC Red synapse. This results in the PC Red firing at a rate higher and essentially decorrelated from the OBJ Red cell. Under this condition, the corresponding synapse will undergo long-term depression ($\approx$t = 170 s in Fig. 6).

The same occurs for the OBJ Blue-PC Blue synapse, as soon as the robot sees the blue object. The perception error signal is reset when the robot reaches the starting point ($\approx t = 220$ s in Fig. 6), and the learning process starts again, first with the blue (blue trace in Fig. 6, at $t\approx$250 s) and then with the cyan object (cyan trace in Fig. 6, at $t> \approx$310 s).

The instantaneous firing rates of all neurons in the network are shown in Fig. 7 A, during one of the three learning cycles represented in Fig. 5. Although we presented these cycles as different attempts of the virtual robot to find an exit (or a special location), it should be noted that they can also be considered as the path that three independent robots may decide to explore. From this point of view, it is then clear that the firing patterns of individual neurons, the time to reach the exit, and the final effective synaptic connectivity, will be in general rather different from each other, although they will end up in carrying out the same cognitive function: just as it will happen for different individuals exploring the same environment. In Fig. 7A we included all neurons in the network, randomly listed, and this gives us the possibility not only to compare our results with experimental data, but also to make experimentally testable predictions. It should be noted that during any given learning trial, and even if the environment is kept the same, each neuron will fire in a rather different way and, in general, an obvious sequence is not evident. Unless the specific role of a given neuron in the network is known, it will be very difficult to understand what is going on. These results are similar to the experimental recordings obtained from a random set of cells while an animal explores an unfamiliar environment, to learn where a reward is, as shown in Fig. 7B (from Dong et al., 2021). The firing rates for another trial are reported in Fig. 7C. In general, the firing rates are highly variable, with many cells exhibiting a substantial amount of bursting behavior, depending on the specific arm that the animal explored. Note that in both Fig. 7 A and 7C there is a cell, identified as cell #23 (Fig. 7 A) and #41 (Fig. 7C), that exhibits a rather regular and high frequency firing for a relatively long time (1–2 min). This firing behavior is not random, but corresponds to the interneuron that is activated by the perception error signal; it informs the network that the robot is in a wrong path. An experimentally testable prediction of the model is thus that, among the many cells firing irregularly, there should be a few with a sustained high frequency firing that code for a wrong location.

Traditionally, the activity of a group of neurons recorded during a typical experiment in which an animal runs down a track or a maze, is visualized by sorting the neurons based on their

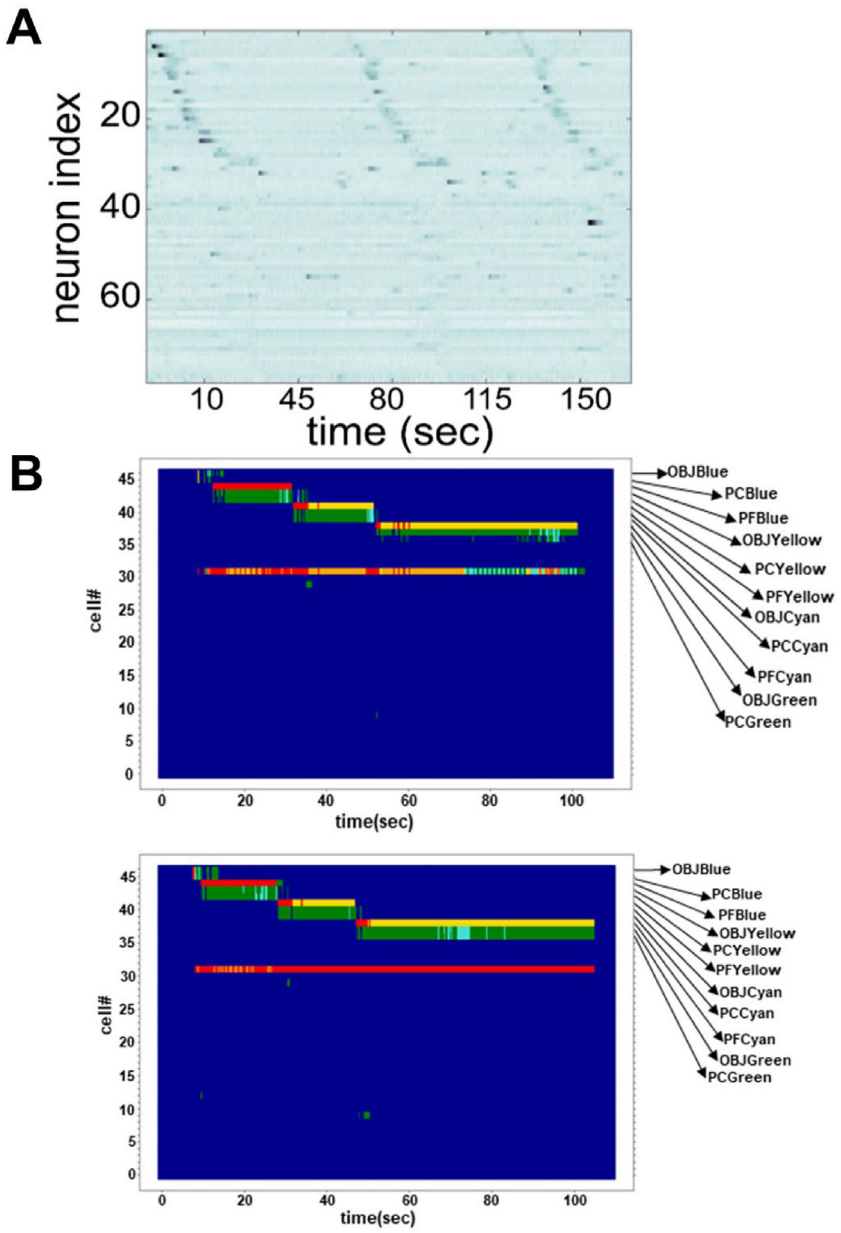

Fig. 8. Network dynamics after a learning trial. (**A**) Typical experimental findings, showing activation of cells with Place and Non-Place-Related activity during three consecutive runs down a linear track, from Meshulam, Gauthier, Brody, Tank, and Bialek (2016); (**B**) Instantaneous firing rate of all cells in the network during two independent runs in the maze after the learning trials of Fig. 7.

average activity, as shown for example in Fig. 8 (top graph, from Meshulam et al., 2016). Cells with place-modulated activity exhibit a characteristic sequential activation correlated with the robot's location in the environment. If we consider the activity of the neurons in our network during the recall phase after the two independent learning trials of Fig. 7 and reorganize the order of the neurons in our network, as shown in the middle and bottom plots of Fig. 8, we can see how a sequential activity naturally emerges from the learning process. Although the actual firing rates may be slightly different after different learning trials (Fig. 8, middle and bottom graphs), as also observed in the experiments, the sequence will be fixed, since it depends on the specific order of objects along the correct path, and their activity will be consistent over a scale of minutes, as also observed experimentally (Liu et al., 2022). The model predicts that, although all neurons involved in the sequence are place-modulated, not all of them are actual Place Cells, but they may also include other neuron types involved in the cognitive process, such as object and/or Persistent Firing cells. Also note the activity of cell #31, which is firing during most of the recall period in both trials, which corresponds to the interneuron sending lateral inhibition to Object cells. The model thus also makes the experimentally testable prediction that neurons firing throughout an entire recall trial in a given experiment are interneurons. Some experimental evidence for this type of activity can be identified for cell #41 in the top panel of Fig. 8.

4. Discussion

In this paper we introduced the e-STL model, a relatively small spiking neuron network architecture able to navigate a maze to learn, during a single learning trial, an arbitrary long series of objects leading to an exit point. It extends the STL model presented in a previous paper (Coppolino et al., 2022),

which suggested the basic neurophysiological mechanisms that can underlie the fast and efficient process of learning an arbitrary sequence of (known) objects. It was a proof of principle, demonstrated in a simplified environment, and it could not work in a more complex environment where, in general, there are dead-ends and/or wrong paths that should be avoided during the recall phase. A typical case is the four-arms maze widely used for *in vivo* experiments. Here, we demonstrated that adding inhibitory neurons (not included in the previous version), gives the network the capacity to find at once a path to reach an exit while forgetting any wrong path explored during the navigation. This ability is crucial to explore complex environments, and we showed how it can emerge from the interplay between interneurons with principal neurons, through well-known physiological mechanisms such as lateral and feedback inhibition. The network elements and connectivity are directly inspired by hippocampal circuitry and, as such, its inner working and performances are entirely explainable from first principles, in contrast with any other traditional artificial intelligence implementations, such as deep learning and Long Short-Term Memory (LSTM) networks. The ability of the e-STL network to learn in a single learning trial and, in doing so, to also explore and eventually forget wrong pathways is especially important.

An LSTM network can use forget gates to explore and dismiss wrong pathways, but the process needs thousands of training epochs to eventually approach (but it will never reach) the optimal result obtained in a single pass by an e-STL network. Other biological inspired models (Whittington et al., 2021, 2020) can achieve extremely good results, but the use of deep learning algorithm for training prevents single shot learning, independently from the feature extraction process (which in our model is hard-coded in the ROS-PYNN interface). In the e-STL model, this can be obtained using a biologically plausible synaptic plasticity rule and interneurons, which have a fundamental role in switching off previously potentiated synapses involved with wrong pathways during the navigation, in a transparent and automatic manner.

The main goal of this work was to show how a cognitive function like spatial navigation can naturally emerge from an extremely fast and optimally efficient self-organization of a relatively simple network based on hippocampal microcircuits. A full-fledged autonomous system able to navigate a complex environment was out of scope, at this stage. The task (navigating a four-arms maze) was chosen because it is a classic experimental environment, almost universally used in *in vivo* experiments to study the neural processes underlying spatial navigation. As long as the problem is to find the correct sequence of objects leading to an exit, the model performances will be the same, no matter how different the environment is; from this point of view, the model is fully general, albeit with the limitations described in the next section. The size of the network was proportionate to the number of predefined objects. It is a modular network, which would linearly grow with the number of objects that it can recognize. Nevertheless, its performances will not depend on size and shape of the environment, or the number of objects in the sequence, because they are related to the way in which each object is progressively linked to the appropriate *HD/PC*s during the learning phase.

Model limitations

One limitation is that the set of objects that can be added to a sequence during the learning phase must be predetermined, i.e. unknown objects will be ignored; this issue can be considered as part of the bigger problem of understanding how the hippocampus is able to generalize and establish new memories on the fly during navigation, extremely more efficiently than any current AI implementation; we will consider this in a future work.

Another apparent limitation is that confusion may arise in learning a sequence containing, for example, multiple instances of the same object in two or more different places. However, it should be noted that this condition can also occur in humans who, especially in the absence of sufficient additional contextual information, may find difficult to decide which object is next in the sequence if there are multiple possibilities.

Finally, another (apparent) limitation is the need for the network to rely on external signals, such as Perception error or visuomotor control. However, one should consider that this is exactly what happens in the real brain, where each region, the hippocampus in our case, continuously receives and sends signals from/to other brain regions specialized in complementary cognitive functions. This approach makes the network ready to be connected and be part of a multi-area model network implementing more complex behaviors.

5. Conclusions

Despite its limitations, it should be clear why an e-STL model may form the basis for a new generation of X-AI applications, in particular for spatial navigation tasks. The network is rather compact, does not need a computationally expensive deep learning algorithm and, in fact, it is always possible to pinpoint and solve a problem arising under special conditions, or figure out where and how to improve or extend its functionalities. At a more general level, the network can be considered as a building block of a larger network including models of other brain regions, providing or receiving preprocessed data. Finally, by following the natural system's layout and circuity, we were able to make several experimentally testable predictions, allowing a deeper and more direct understanding of the mechanism underlying cognitive functions and dysfunctions. Future extensions will consider additional processes, naturally occurring in the hippocampal network, such as continuous learning and recall and the ability to form new memories during navigation.

Declaration of competing interest

The authors declare that they have no known competing financial interests or personal relationships that could have appeared to influence the work reported in this paper.

Data availability

Complete source code and demo will be publicly available on the Neurorobotics Platform of EBRAINS and ModelDB.

Acknowledgments

This work was supported by the European Union's Horizon 2020 Framework Program for Research and Innovation under the Specific Grant Agreement 945539 (Human Brain Project SGA3). We thank Annemieke Michels (EBRAINS) for editorial assistance, and by the Italian National Recovery and Resilience Plan (NRRP), M4C2, funded by the European Union – NextGenerationEU (Project IR0000011, CUP B51E22000150006, EBRAINS-Italy).

Appendix A. Supplementary data

Supplementary material related to this article can be found online at https://doi.org/10.1016/j.neunet.2023.03.030.

References

Abadi, M., et al. (2015). *TensorFlow: Large-scale machine learning on heterogeneous system*. [Online] Available: https://tensorflow.org.

Aika, Y., Ren, J. Q., Kosaka, K., & Kosaka, T. (1994). Quantitative analysis of GABA-like-immunoreactive and parvalbumin-containing neurons in the CA1 region of the rat hippocampus using a stereological method, the disector. *Experimental Brain Research*, *99*(2), 267–276. http://dx.doi.org/10.1007/BF00239593, PMID: 7925807.

Arleo, A., & Gerstner, W. (2000). Spatial cognition and neuro-mimetic navigation: a model of hippocampal place cell activity. *Biological Cybernetics*, *83*(3), 287–299. http://dx.doi.org/10.1007/s004220000171, PMID: 11007302.

Boran, E., Fedele, T., Klaver, P., Hilfiker, P., Stieglitz, L., Grunwald, T., et al. (2019). Persistent hippocampal neural firing and hippocampal-cortical coupling predict verbal working memory load. *Science Advances*, *5*(3), eaav3687. http://dx.doi.org/10.1126/sciadv.aav3687.

Brette, R., Rudolph, M., Carnevale, T., et al. (2007). Simulation of networks of spiking neurons: a review of tools and strategies. *Journal of Computational Neuroscience*, *23*(3), 349–398. http://dx.doi.org/10.1007/s10827-007-0038-6.

Brownlee, J. (2018). *Deep learning for time series forecasting*.

Brunel, N. (2000). Dynamics of sparsely connected networks of excitatory and inhibitory spiking neurons. *Journal of Computational Neuroscience*, *8*, 183–208.

Cessac, Bruno, & Viéville, Thierry (2008). On dynamics of integrate-and-fire neural networks with conductance based synapses. *Frontiers in Computational Neuroscience*, http://dx.doi.org/10.3389/neuro.10.002.2008.

Chollet, F. (2015). *Keras*. [Online] Available: https://keras.io.

Coppolino, S., Giacopelli, G., & Migliore, M. (2022). Sequence learning in a single trial: A spiking neurons model based on hippocampal circuitry. In *IEEE transactions on neural networks and learning systems*. http://dx.doi.org/10.1109/TNNLS.2021.3049281.

Danjo, T. (2020). Allocentric representations of space in the hippocampus. *Neuroscience Research*, *153*, 1–7. http://dx.doi.org/10.1016/j.neures.2019.06.002, Epub 2019 Jul 2. PMID: 31276699.

Davison, A. P., Brüderle, D., Eppler, J. M., Kremkow, J., Muller, E., Pecevski, D. A., et al. (2009). PyNN: a common interface for neuronal network simulators. *Frontiers in Neuroinformatics*, *2*(11).

Diamond, Jeffrey S. (2017). *Inhibitory interneurons in the retina: types, circuitry, and function*. http://dx.doi.org/10.1146/annurev-vision-102016-061345.

Dong, C., Madar, A. D., & Sheffield, M. E. J. (2021). Distinct place cell dynamics in CA1 and CA3 encode experience in new environments. *Nature Communications*, *12*(1), 2977. http://dx.doi.org/10.1038/s41467-021-23260-3, PMID: 34016996; PMCID: PMC8137926.

Ferrante, M., Migliore, M., & Ascoli, G. A. (2009). Feed-forward inhibition as a buffer of the neuronal input–output relation. *Proceedings of the National Academy of Sciences of the United States of America (Washington, DC)*, *106*(42), 18004–18009. http://dx.doi.org/10.1073/pnas.0904784106, Epub 2009 Oct 8. PMID: 19815518; PMCID: PMC2764942.

Franck, J. E., Pokorny, J., Kunkel, D. D., & Schwartzkroin, P. A. (1995). Physiologic and morphologic characteristics of granule cell circuitry in human epileptic hippocampus. *Epilepsia*, *36*(6), 543–558. http://dx.doi.org/10.1111/j.1528-1157.1995.tb02566.x; (1995). Erratum. *Epilepsia*, *36*(10), 1064, PMID: 7555966.

Gulli, R. A., Duong, L. R., Corrigan, B. W., Doucet, G., Williams, S., Fusi, S., et al. (2020). Context-dependent representations of objects and space in the primate hippocampus during virtual navigation. *Nature Neuroscience*, *23*(1), 103–112. http://dx.doi.org/10.1038/s41593-019-0548-3, Epub 2019 Dec 23. PMID: 31873285.

Gunning, D., Stefik, M., Choi, J., Miller, T., Stumpf, S., & Yang, G. Z. (2019). XAI-explainable artificial intelligence. *Science Robotics*, *4*(37), eaay7120. http://dx.doi.org/10.1126/scirobotics.aay7120, PMID: 33137719.

Johnson, N. L., Kemp, A. W., & Kotz, S. (2005). Poisson distribution. In *Univariate discrete distributions* (3rd ed.). (pp. 156–207). New York, NY, USA: Wiley, http://dx.doi.org/10.1002/0471715816.

Knopp, A., Kivi, A., Wozny, C., Heinemann, U., & Behr, J. (2005). Cellular and network properties of the subiculum in the pilocarpine model of temporal lobe epilepsy. *Journal of Comparative Neurology*, *483*(4), 476–488. http://dx.doi.org/10.1002/cne.20460, PMID: 15700275.

Leutgeb, S., Ragozzino, K. E., & Mizumori, S. J. (2000). Convergence of head direction and place information in the CA1 region of hippocampus. *Neuroscience*, *100*(1), 11–19. http://dx.doi.org/10.1016/s0306-4522(00)00258-x, PMID: 10996454.

Liu, Y., Levy, S., Mau, W., Geva, N., Rubin, A., Ziv, Y., et al. (2022). Consistent population activity on the scale of minutes in the mouse hippocampus. *Hippocampus*, http://dx.doi.org/10.1002/hipo.23409, Epub ahead of print. PMID: 35225408.

Lübke, J., Markram, H., Frotscher, M., & Sakmann, B. (1996). Frequency and dendritic distribution of autapses established by layer 5 pyramidal neurons in the developing rat neocortex: comparison with synaptic innervation of adjacent neurons of the same class. *Journal of Neuroscience*, *16*(10), 3209–3218. http://dx.doi.org/10.1523/JNEUROSCI.16-10-03209.1996.

Meshulam, Leenoy, Gauthier, Jeffrey, Brody, Carlos, Tank, David, & Bialek, William (2016). Collective behavior of place and non-place neurons in the hippocampal network. *Neuron*, 96. http://dx.doi.org/10.1016/j.neuron.2017.10.027.

Migliore, M., Novara, G., & Tegolo, D. (2008). Single neuron binding properties and the magical number 7. *Hippocampus*, *18*(11), 1122–1130. http://dx.doi.org/10.1002/hipo.20480, PMID: 18680161.

Nishiyama, M., Hong, K., Mikoshiba, K., Poo, M. M., & Kato, K. (2000). Calcium stores regulate the polarity and input specificity of synaptic modification. *Nature*, *408*, 584–588.

Nordlie, E., Tetzlaff, T., & Einevoll, G. T. (2010). Rate dynamics of leaky integrate-and-fire neurons with strong synapses. http://dx.doi.org/10.3389/fncom.2010.00149.

O'Keefe, J., & Dostrovsky, J. (1971). The hippocampus as a spatial map. Preliminary evidence from unit activity in the freely-moving rat. *Brain Research*, *34*(1), 171–175. http://dx.doi.org/10.1016/0006-8993(71)90358-1, PMID: 5124915.

Quiroga, R. Q., Reddy, L., Kreiman, G., Koch, C., & Fried, I. (2005). Invariant visual representation by single neurons in the human brain. *Nature*, *435*(7045), 1102–1107.

Schmidhuber, J. (2015). Deep learning in neural networks: an overview. *Neural Networks*, *61*, 85–117.

Schoppa, N. E., & Westbrook, G. L. (2002). AMPA autoreceptors drive correlated spiking in olfactory bulb glomeruli. *Nature Neuroscience*, *5*(11), 1194–1202. http://dx.doi.org/10.1038/nn953.PMID:12379859.

Strösslin, T., Sheynikhovich, D., Chavarriaga, R., & Gerstner, W. (2005). Robust self-localisation and navigation based on hippocampal place cells. *Neural Networks*, *18*(9), 1125–1140. http://dx.doi.org/10.1016/j.neunet.2005.08.012, Epub 2005 Nov 2. PMID: 16263241.

Sutton, R. S., & Barto, A. G. (2018). *Reinforcement learning: an introduction*. The MIT Press.

Van der Loos, H., & Glaser, E. M. (1972). Autapses in neocortex cerebri: synapses between a pyramidal cell's axon and its own dendrites. *Brain Research*, *48*, 355–360. http://dx.doi.org/10.1016/0006-8993(72)90189-8, PMID: 4645210.

Whittington, James C. R., Warren, Joseph, & Behrens, Tim. E. J. (2021). Relating transformers to models and neural representations of the hippocampal formation. In *International conference on learning representations*.

Whittington, James C. R., et al. (2020). The Tolman–Eichenbaum machine: unifying space and relational memory through generalization in the hippocampal formation. *Cell*, *183*(5), 1249–1263.

Woodson, W., Nitecka, L., & Ben-Ari, Y. (1989). Organization of the GABAergic system in the rat hippocampal formation: a quantitative immunocytochemical study. *Journal of Comparative Neurology*, *280*(2), 254–271. http://dx.doi.org/10.1002/cne.902800207.PMID:2925894.

Yokoi, M., Mori, K., & Nakanishi, S. (1995). Refinement of odor molecule tuning by dendrodendritic synaptic inhibition in the olfactory bulb. *Proceedings of the National Academy of Sciences of the United States of America (Washington, DC)*, *92*, 3371–3375.

Zeno, Peter, Patel, Sarosh, & Sobh, Tarek (2016). Review of neurobiologically based mobile robot navigation system research performed since 2000. *Journal of Robotics*, *2016*, 1–17. http://dx.doi.org/10.1155/2016/8637251.